IEEE Access
Multidisciplinary ⋮ Rapid Review ⋮ Open Access Journal

Received October 29, 2020, accepted November 4, 2020, date of publication November 9, 2020, date of current version November 19, 2020.

Digital Object Identifier 10.1109/ACCESS.2020.3036643

Performance of Generalized QAM/FSO Systems With Pointing Misalignment and Phase Error Over Atmospheric Turbulence Channels

THANG V. NGUYEN[1], (Graduate Student Member, IEEE), THANH V. PHAM[1], (Member, IEEE), NGOC T. DANG[1,2], (Member, IEEE), AND ANH T. PHAM[1], (Senior Member, IEEE)

[1]Computer Communications Laboratory, The University of Aizu, Aizuwakamatsu 965-8580, Japan
[2]Posts and Telecommunications Institute of Technology, Hanoi 100000, Vietnam

Corresponding author: Anh T. Pham (pham@u-aizu.ac.jp)

This work was supported by the Vietnam National Foundation for Science and Technology Development (NAFOSTED) under Grant 102.02-2019.08.

ABSTRACT This article investigates the performance of free-space optical (FSO) systems using sub-carrier quadrature amplitude modulation (SC-QAM) signaling for broadband terrestrial applications. While previous studies ignored the influence of phase noise, we theoretically analyze and derive closed-form expressions of the system's average bit error rate (ABER) considering the combined effect of pointing misalignment, turbulence-induced fading, and phase error. The log-normal distribution is used to model the atmospheric turbulence in the weak regime while the gamma-gamma distribution is applied for modeling the turbulent atmosphere in the moderate and strong regimes. The phase error, which becomes complicated under the effect of atmospheric turbulence, is modeled by Tikhonov distribution. The numerical results reveal that the influence of the phase error on the system performance is dominant in the weak turbulence and high order modulation while the fading becomes more severe in the moderate-to-strong turbulence regime. The accuracy of analytical results is also validated by Monte-Carlo simulations and a good match can be confirmed.

INDEX TERMS Free-space optics (FSO), quadrature-amplitude modulation (QAM), log-normal distribution, gamma-gamma distribution, phase error, pointing misalignment.

I. INTRODUCTION

Over the past decade, the ever-increasing demand for high-speed wireless applications has been resulting in the spectrum congestion problem in radio frequency (RF) communications [1]. To address this issue, optical wireless technologies such as free-space optical (FSO) communications have been becoming a promising alternative due to their operation over unlicensed spectrum [2]–[5]. Being able to support Gbps data rates, FSO systems can facilitate Internet access to remote areas where installing wired connections is costly and/or time-consuming.

Operating over the free-space medium, the performance of terrestrial FSO systems is significantly affected by atmospheric conditions. On the one hand, it is the power loss due to absorption and scattering by particles (e.g. water droplets, dust, and snow) in the air. This essentially limits the coverage of the systems. On the other hand, it is the random fluctuation of transmitted optical power (intensity) caused by atmospheric turbulence, which is a result of changes in the refractive index due to inhomogeneity in temperature and pressure. As a matter of fact, there have been a number of studies on turbulence-induced fading mitigation methods for FSO systems, notably diversity and relaying techniques [6]–[9].

Conventional FSO systems predominately employ intensity modulation/direct detection (IM/DD) scheme, where the information bits are encoded by the intensity of the transmitted laser beam. The most commonly implemented IM technique is on-off keying (OOK) thanks to its simplicity. For optimal signal detection in the presence of atmospheric turbulence, an adaptive thresholding scheme, which requires

The associate editor coordinating the review of this manuscript and approving it for publication was Xiaofei Wang.

This work is licensed under a Creative Commons Attribution 4.0 License. For more information, see https://creativecommons.org/licenses/by/4.0/

instantaneous channel fading knowledge, is needed at the receiver. This consequently increases the receiver complexity. Additionally, OOK offers lower energy and spectral efficiency. To address these drawbacks of OOK, pulse-position modulation (PPM) is a possible alternative as it does not need adaptive thresholding and is more energy-efficient [10], [11]. However, PPM also exhibits poor spectral efficiency. These limitations of OOK and PPM have motivated extensive research on subcarrier intensity modulation (SIM), which is able to support high data-rates with cost-effective implementation [12]–[17]. The adoption of this modulation scheme is also encouraged to seamlessly integrate FSO systems into current fiber optics networks, where SIMs are already commercially deployed. The use of SIM can enable both coherent and noncoherent modulation schemes, where the former is preferable due to its better bit error rate (BER) performance. For the coherent modulation, a carrier phase recovery is required at the receiver to achieve the optimal performance. The phase recovery process is, nonetheless, sensitive to noise and turbulence-induced fading. As such, errors in carrier phase estimation (CPE) are inevitable. Even in noncoherent modulation systems where there is no need for phase recovery, phase errors can still be generated due to hardware impairments [18], [19].

Although the impact of turbulence-induced fading on the performance of SIM/FSO has been extensively investigated, such studies for the case of phase errors are rather scarce. The error performances of subcarrier phase-shift keying (PSK) FSO systems with phase errors being modeled as a Tikhonov distribution were first studied in [20] and [21] for log-normal and gamma-gamma turbulence channel, respectively. In the case of the log-normal channel, asymptotic noise reference loss expressions were derived to quantify the performance degradation caused by phase errors. It was shown that while the impact of phase errors on binary phase-shift keying (BPSK) systems was negligible; it could not be ignored in the case of higher-order PSK. For the gamma-gamma channel, closed-form expressions for the average symbol error probability (ASEP) were derived in the case of BPSK with a negligible phase error effect. For the general case, since closed-form solutions were not possible, an approximation to the Tikhonov distribution was introduced to facilitate the analysis. For the case of SIM with noncoherent modulation, the authors in [22] examined ASEP of FSO systems using M-ary differential phase-shift keying (MDPSK) over gamma-gamma channel with pointing errors. Instead of using the approximation method proposed in [21], the probability density function (PDF) of the Tikhonov distribution was represented by its Fourier series expansion, leading to a convergent series expression for the ASEP. Numerical results revealed that the presence of phase errors could result in an unrecoverable error-rate floor, which is a limiting factor of SIM-DPSK FSO systems. Extending the single-input single-output (SISO) configuration considered in previous works, approximate ASEP expressions for single-input single-output and single-input multiple-output (SIMO) links were presented in [23].

It is worth noting that all above-mentioned studies attempted to explore the impact of phase errors on SIM/FSO systems using PSK or its variants. While PSK is suitable for long-range communications such as satellite links where channel robustness is of importance, it suffers from low spectral efficiency [24], [25]. In this regard, the spectrally efficient QAM is preferable as both amplitude and phase are modulated. As a matter of fact, QAM is a family of modulations with different constellation types corresponding to different arrangements of the signal points [26]. While square QAM (a special case of the rectangular QAM) is widely deployed in terrestrial wireless standards such as wireless fidelity (Wi-Fi), and 3G/4G/5G cellular networks, star QAM is used in the satellite communication standards such as Digital Video Broadcast System (DVB) S2, DVB-SH, Internet Protocol over Satellite (IPoS), and Advanced Broadcasting Systems via Satellite (ABS-S) [27], [28]. On the other hand, cross QAM is useful in adaptive modulation schemes and is adopted in various systems such as Asymmetric Digital Subscribers Line (ADSL), Very high-speed Digital Subscriber Line (VDSL), and Digital Video Broadcasting - Cable (DVB-C) [29]. Considering that rectangular QAM is a generalization of the square one, which is the most commonly used variant, this article focuses on the performance analysis of FSO systems using rectangular QAM.

There have been several investigations on the performance of SIM-QAM FSO systems over the past decade. Using an exponential approximation to the Gaussian Q-function, the approximate ASEPs of a SIM/FSO system employing general order rectangular QAM were evaluated over log-normal and gamma-gamma turbulence channels in [30]. Exact ASEP expressions were obtained in [31] for gamma-gamma, K-distributed, and negative exponential channels using a series expansion of the modified Bessel function. Considering BER as the performance metric, the authors in [32] examined a general rectangular QAM/FSO system using an avalanche photodiode (APD) over gamma-gamma channels. The impact of signal-dependent receiver noise was also taken into account. Recently, a hybrid QAM-multi-pulse pulse-position modulation (MPPM) has been proposed and studied to improve the power efficiency compared to the traditional QAM [33], [34]. Comparisons between QAM and other modulation schemes in terms of BER and outage probability can be found in [35].

To the best of the authors' knowledge, aside from the conference version of this article [36], there has been no study on the performance analysis of SIM-QAM FSO systems considering the impact of phase errors in the literature. It has been shown in previous works that the influence of phase errors is proportional to the modulation order in the case of PSK. Hence, it is also expected that the performance degradation caused by phase errors in the case of QAM would be significant as high-order QAM is usually employed to

provide high data-rates. In our previous study, we presented an ASEP analysis for the special case of square QAM with gamma-gamma turbulence channel and phase errors. Based on the obtained initial results, this article attempts to provide a comprehensive performance analysis for SIM-QAM FSO systems with phase errors, which is summarized as follows

- We examine a more general channel model, which, in addition to turbulence-induced fading and phase errors, takes pointing misalignment into account. In practical FSO systems, pointing misalignment due to transceiver vibration and/or building sway is inevitable and results in a considerable reduction in the received optical power [37], [38].
- Instead of ASEP and square QAM as being considered in the conference version, we derive closed-form expressions for the average BER (ABER), which is a better indicator of the system performance, considering general rectangular QAM with Gray coding. It should be noted that while an exact closed-form expression of BER for the general rectangular QAM over additive white Gaussian noise (AWGN) channel was presented in [39], the derivation is not applicable to the case with phase errors. By characterizing a detection rule for each bit in the QAM symbol, we newly derived approximate closed-form expressions for the ABER of the considered system over log-normal and gamma-gamma turbulence channels.

The remainder of the paper is organized as follows. The system and channel model are described in Section II. The bit detection rule and ABER analysis are presented in Section III. Representative numerical results are displayed and discussed in Section IV. Finally, we conclude the paper in Section V.

II. SYSTEM AND CHANNEL MODEL

A. SYSTEM MODEL

We consider in this article an FSO system employing general rectangular M-ary QAM. At the transmitter, each block of $\log_2 M$ information bits is firstly modulated into a QAM symbol by an I-Q modulator, where I and Q are the in-phase and quadrature, respectively. The output signal of the modulator can be represented by

$$s_m(t) = A_{mI}\, g(t) \cos(2\pi f_c t) - A_{mQ} g(t) \sin(2\pi f_c t), \quad (1)$$

where A_{mI} and A_{mQ} $(m = 1, 2, \ldots, M)$ are the amplitudes of data-bearing signals with respect to the I and Q channel, respectively. $g(t)$ is the shaping pulse, f_c is the subcarrier frequency. The electrical QAM signal is then used to modulate the intensity of an optical beam, which can be expressed as

$$s(t) = P_s\left(1 + \delta s_m(t)\right), \quad (2)$$

where $0 < \delta < 1$ is the modulation index and P_s is the power of the transmitted optical signal. The received optical intensity at the input of a PIN photodiode is given by

$$r(t) = hP_s\Big(1 + \delta\big(A_{mI} g(t) \cos(2\pi f_c t + \theta_e) - A_{mQ} g(t) \sin(2\pi f_c t + \theta_e)\big)\Big), \quad (3)$$

where the channel coefficient, $h = h_l h_a h_p$, composes of geometrical path loss h_l, atmospheric turbulence-induced fading h_a modeled by the log-normal distribution in weak turbulence and gamma-gamma distribution in the strong turbulence regime, and the pointing error h_p. Additionally, θ_e denotes the turbulence-induced phase error, which is modeled by the Tikhonov distribution.

The electrical signal at the output of the photodiode after the DC bias term being filtered out is then expressed by

$$r_e(t) = h\Re P_s\delta\big(A_{mI} g(t) \cos(2\pi f_c t + \theta_e) - A_{mQ} g(t) \sin(2\pi f_c t + \theta_e)\big) + n(t), \quad (4)$$

where $n(t)$ denotes a zero-mean AWGN whose variation $\sigma_n^2 = N_0/2$ with N_0 being the noise power spectral density and $\Re$ is the responsivity of the photodiode. Accordingly, the instantaneous electrical signal-to-noise ratio (SNR) per symbol at the output of the receiver is given by

$$\gamma = \frac{(\delta\Re P_s h)^2}{\sigma_n^2}, \quad (5)$$

To facilitate the performance analysis of high-order modulation schemes like QAM, it is common to use the SNR per bit, which is

$$\gamma_b = \frac{\gamma}{\log_2(M)}, \quad (6)$$

where M is the modulation order. The average SNR per bit is then $\bar{\gamma}_b = \mathbb{E}[\gamma_b] = \frac{(\delta\Re P_s)^2 \mathbb{E}(h^2)}{\log_2 M \sigma_n^2}$.

B. CHANNEL MODEL

In terrestrial FSO systems, the propagation of an optical signal is mainly affected by three key factors, including path loss, atmospheric turbulence-induced phase error and fading, and pointing misalignment. Hence, the composite channel coefficient h can be formulated as

$$h = h_l h_p h_a, \quad (7)$$

where h_l is the path loss, which is dependent on the transmission distance and weather condition. h_p represents the power loss due to transceiver pointing misalignment and is characterized by a random variable. Finally, h_a is also a random variable, which describes the fading caused by intensity fluctuations of the optical beam propagating through atmospheric turbulence channel.

1) PATH LOSS (h_l)

The path loss is commonly modeled by the Beers-Lambert law as follows

$$h_l = \exp(-\alpha_l L), \quad (8)$$

where L is the transmission distance and α_l is the attenuation coefficient, which is weather-dependent. Some typical values of α_l corresponding to different weather conditions are shown in Table 1.

TABLE 1. Typical values of the attenuation coefficient [40].

Weather conditions	α_l (dB/km)
Heavy fog	125
Light fog	20
Heavy rain	9.2
Moderate rain	5.8
Haze	4.2
Clear air	0.43

2) POINTING MISALIGNMENT (h_p)

Mechanical errors and/or transceiver vibration due to for example strong wind, building sway might cause pointing misalignments, which further results in power loss at the receiver. Geometrically shown in Fig. 1, the pointing misalignment is characterized by vector $\mathbf{r}_e$ from the center of the photodetector to that of the beam footprint. At the transmission distance L, the fraction of power collected at the photodetector is given by [37]

$$h_p(r_e, L) \approx A_0 \exp\left(-\frac{2r_e^2}{w_{L_{\text{eq}}}^2}\right), \tag{9}$$

where $r_e = \|\mathbf{r}_e\|$, $A_0 = (\text{erf}(\nu))^2$ is the fraction of collected power at $L = 0$, and $w_{L_{\text{eq}}}^2 = \frac{w_L^2\sqrt{\pi}\text{erf}(\nu)}{2\nu\exp(-\nu^2)}$ is the equivalent beam width with $\nu = \frac{\sqrt{\pi}a}{\sqrt{2}w_L}$ and a being the radius of photodetector aperture. w_L denotes the beam waist of a Gaussian beam propagating through an atmospheric turbulence channel. At the channel distance L, it can be approximated by $w_L \approx w_o\left[1 + \varepsilon\left(\frac{\lambda L}{\pi w_o^2}\right)^2\right]^{\frac{1}{2}}$, where w_0 is the beam waist at $L = 0$ (i.e. at the transmitter), λ is the optical wavelength, $\varepsilon = 1 + \frac{2w_o^2}{\rho_0^2(z)}$ with $\rho_0(z) = (0.55C_n^2k^2L)^{-3/5}$ being the coherence length, C_n^2 being the refractive index structure parameter, and $k = \frac{2\pi}{\lambda}$ being the optical wave number.

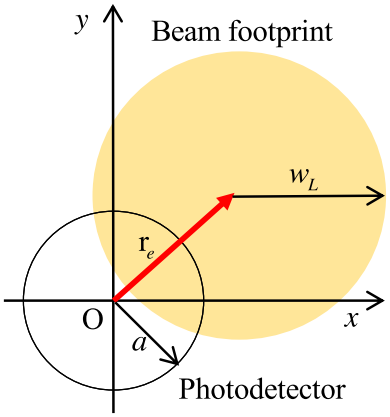

FIGURE 1. Misalignment between Gaussian beam footprint and detector at the receiver lens area.

Assume that the radial distance r_e is random and modeled by a Rayleigh distribution with the scale parameter σ_p being the jitter standard deviation at the receiver, the probability density distribution (PDF) of h_p can be written as [37]

$$f_{h_p}(h_p) = \frac{\xi^2}{A_0^{\xi^2}} h_p^{\xi^2-1}, \quad 0 \le h_p \le A_0, \tag{10}$$

where $\xi = \frac{w_{L_{\text{eq}}}}{2\sigma_p}$.

3) ATMOSPHERIC TURBULENCE-INDUCED FADING (h_a)

In addition to geometrical path loss, the atmospheric channel also causes random fluctuations in the transmitted beam intensity, which results in signal fade at the receiver. For the sake of performance analysis, a number of distribution models have been proposed to describe this turbulence-induced fading. It is well-known that the log-normal distribution is sufficient and mathematically simple in the case of weak turbulence. Assume that the fading power is normalized to unity, its PDF following the log-normal distribution is given by

$$f_{h_a}(h_a) = \frac{1}{h_a\sigma_s\sqrt{2\pi}} \exp\left[-\frac{\left(\ln(h_a) + \frac{\sigma_s^2}{2}\right)^2}{2\sigma_s^2}\right], \tag{11}$$

in which σ_s^2 is the log-intensity variance given as

$$\sigma_s^2 = \exp\left[\frac{0.49\sigma_R^2}{\left(1 + 0.18z_L^2 + 0.56\sigma_R^{12/5}\right)^{7/6}} + \frac{0.51\sigma_R^2}{\left(1 + 0.9z_L^2 + 0.62\sigma_R^{5/6}\right)^{5/6}}\right] - 1, \tag{12}$$

where $z_L = \sqrt{ka^2/L}$ and σ_R^2 is the Rytov variance [15]. In the case of plane wave propagation, σ_R^2 is given by

$$\sigma_R^2 = 1.23k^{7/6}C_n^2L^{11/6}. \tag{13}$$

Combining (8), (10), and (11), the distribution of h can be derived as [41]

$$f_h(h) = \frac{\xi^2}{2(A_0h_l)^{\xi^2}} h^{\xi^2-1} \exp\left[2\sigma_s^2\xi^2\left(1 + \xi^2\right)\right] \times \text{erfc}\left[\frac{\ln\left(\frac{h}{A_0h_l}\right) + 2\sigma_s^2\left(1 + 2\xi^2\right)}{\sqrt{8\sigma_s^2}}\right], \tag{14}$$

where erfc(·) is the complementary error function. Accordingly, after some simple manipulation, we can get the PDF of the instantaneous SNR per bit γ_b as

$$f_{\gamma_b}(\gamma_b) = \frac{\xi^2}{4(A_0h_l)^{\xi^2}} \frac{\gamma_b^{\frac{\xi^2}{2}-1}}{\bar{\gamma}_b^{\frac{\xi^2}{2}}} \exp\left[2\sigma_s^2\xi^2\left(1+\xi^2\right)\right] \times \text{erfc}\left[\frac{\ln\left(\frac{1}{A_0h_l}\sqrt{\frac{\gamma_b}{\bar{\gamma}_b}}\right) + 2\sigma_s^2\left(1 + 2\xi^2\right)}{\sqrt{8\sigma_s^2}}\right]. \tag{15}$$

To characterize a wide range of turbulence strength, the gamma-gamma distribution is commonly used due to its mathematical tractability [42]. The PDF of the fading power following gamma-gamma distribution is given by

$$f_{h_a}(h_a) = \frac{2(\alpha\beta)^{(\alpha+\beta)/2}}{\Gamma(\alpha)\Gamma(\beta)} h_a^{\frac{\alpha+\beta}{2}-1} K_{\alpha-\beta}\left(2\sqrt{\alpha\beta h_a}\right), \quad (16)$$

where $K_{\alpha-\beta}(\cdot)$ is the modified Bessel function of the second kind and order $(\alpha-\beta)$ and $\Gamma(\cdot)$ denotes the gamma function. α and β are the effective numbers of large-scale and small-scale turbulences. In the case of zero-inner scale, they are given by

$$\alpha = \left\{ \exp\left[\frac{0.49\sigma_R^2}{\left(1+1.11\sigma_R^{12/5}\right)^{7/6}} \right] - 1 \right\}^{-1}, \quad (17)$$

$$\beta = \left\{ \exp\left[\frac{0.51\sigma_R^2}{\left(1+0.69\sigma_R^{12/5}\right)^{5/6}} \right] - 1 \right\}^{-1}. \quad (18)$$

Similar to the case of log-normal distribution, the PDFs of h and γ_b are derived as [43]

$$f_h(h) = \frac{\alpha\beta\xi^2}{A_0 h_l \Gamma(\alpha)\Gamma(\beta)} \times G_{1,3}^{3,0}\left[\frac{\alpha\beta}{A_0 h_l} h \middle| \begin{matrix} \xi^2 \\ \xi^2-1, \alpha-1, \beta-1 \end{matrix} \right], \quad (19)$$

and

$$f_{\gamma_b}(\gamma_b) = \frac{\xi^2}{2\gamma_b \Gamma(\alpha)\Gamma(\beta)} G_{1,3}^{3,0}\left[\frac{\alpha\beta\xi^2}{\xi^2+1}\sqrt{\frac{\gamma_b}{\overline{\gamma}_b}} \middle| \begin{matrix} \xi^2+1 \\ \xi^2, \alpha, \beta \end{matrix} \right], \quad (20)$$

respectively, where $G_{p,q}^{m,n}[\cdot|\cdot]$ denotes the Meijer G-function [44].

C. PHASE ERROR MODEL

At the receiver, the CPE is performed using a phase-locked loop (PLL). In the presence of noise and turbulence-induced fading, an estimation error might occur, which further deteriorates the system performance. It has been shown that the phase error follows a Tikhonov distribution, whose conditional PDF is given by [45]

$$f_{\theta_e|\rho}(\theta_e|\rho) = \frac{\exp(\rho\cos\theta_e)}{2\pi I_0(\rho)}, \quad -\pi \le \theta_e \le \pi \quad (21)$$

where $I_0(\cdot)$ is the zero-order first kind modified Bessel function and ρ is the SNR of the PLL used for carrier synchronization. It is observed that ρ is proportional to the instantaneous SNR per bit γ_b as $\rho = C\gamma_b$, where C is a constant whose typical value is around 10 [20]. Hence, (21) can be rewritten as

$$f_{\theta_e|\gamma_b}(\theta_e|\gamma_b) = \frac{\exp(C\gamma_b\cos\theta_e)}{2\pi I_0(C\gamma_b)}, \quad -\pi \le \theta_e \le \pi. \quad (22)$$

III. AVERAGE BIT ERROR RATE

In this section, we focus on deriving the ABER of the considered system using general-order rectangular $M_I \times M_Q$ QAM (i.e. $M = M_I \times M_Q$) by characterizing a decision rule for each bit of a QAM symbol. For this purpose, we first examine an example for the specific case of 8×4 QAM. The decision rule and ABER expressions for the general case are then developed.

A. BIT DECISION RULE

Figure 2 shows the signal space diagram of an 8×4 QAM represented in a two-dimensional Cartesian system, where the two axes are the I and Q channel. Essentially, the signal constellation of an $M_I \times M_Q$ QAM can be seen as a combination of two pulse amplitude modulation (PAM) signalings (i.e. M_I-ary and M_Q-ary PAM). In our example 8×4 QAM scheme, the I channel represents an 8-PAM whose symbols are constituted of 3 bits (i_1, i_2, i_3) while the Q channel is a 4-PAM whose symbols consist of 2 bits (q_1, q_2). In addition, data bits on each channel are mapped into the constellation point by using Gray coding and all symbols are assumed to be equally likely transmitted.

To facilitate the calculation of bit error probability, it is beneficial to represent each received symbol by its coordinate in the defined Cartesian system as illustrated in Fig. 3. Denote S_m as the original symbol under the ideal condition (i.e. no noise and phase error) whose coordinate is $(r_{mI}, r_{mQ}) = (A_{mI}d_I, A_{mQ}d_Q)$, where d_I and d_Q are the in-phase and quadrature half decision distances, respectively [36]. The coordinate (r'_{mI}, r'_{mQ}) of symbol S'_m, which corresponds to S_m impaired by phase error θ_e and the noise vector $\mathbf{n}$, can then be expressed by

$$r'_{mI} = A_{mI}d_I\cos(\theta_e) - A_{mQ}d_I\sin(\theta_e) + n, \quad (23a)$$

$$r'_{mQ} = A_{mI}d_Q\sin(\theta_e) + A_{mQ}d_Q\cos(\theta_e) + n. \quad (23b)$$

For a general $M_I \times M_Q$ QAM, in-phase and quadrature half decision distances are given by

$$\frac{d_I}{\sqrt{2\sigma_n^2}} = \sqrt{\frac{3\log_2(M)\gamma_b}{\left(M_I^2-1\right)+r^2\left(M_Q^2-1\right)}}, \quad (24)$$

$$\frac{d_Q}{\sqrt{2\sigma_n^2}} = \sqrt{\frac{3r^2\log_2(M)\gamma_b}{\left(M_I^2-1\right)+r^2\left(M_Q^2-1\right)}}. \quad (25)$$

where $r = \frac{d_Q}{d_I}$ is the quadrature-to-inphase decision distance ratio. Without loss of generality, assume that $r = 1$, resulting in $d_I = d_Q = d$.

For a better explanation, let us characterize the bit error conditions on the I and Q channel separately. For the I channel, as shown in Fig. 4, the boundary decision of each bit i_1, i_2, and i_3 is defined based on the position of the symbol which contains the bit. Specifically, bit i_1 decision is made according to

$$i_1 = \begin{cases} 1 & if \ \ r'_{mI} < 0, \\ 0 & if \ \ r'_{mI} \ge 0. \end{cases} \quad (26)$$

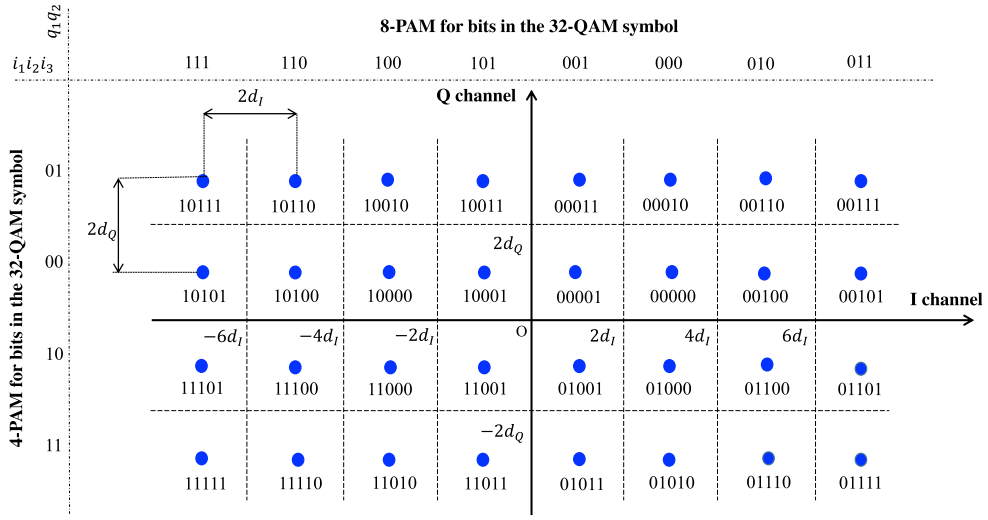

FIGURE 2. Signal space diagram for the 8 ×4 QAM scheme.

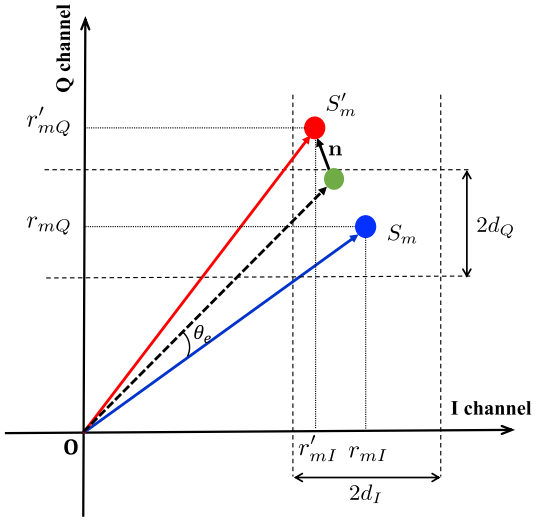

FIGURE 3. Illustration of bit errors due to AWGN and phase error.

In a similar way, the decisions for bit i_2 and i_3 are shown as

$$i_2 = \begin{cases} 1 & \text{if } r'_{mI} < -4d \text{ or } r'_{mI} \geq 4d, \\ 0 & \text{if } -4d \leq r'_{mI} < 4d, \end{cases} \tag{27}$$

and

$$i_3 = \begin{cases} 1 & \text{if } r'_{mI} < -6d \text{ or } -2d \leq r'_{mI} < 2d \\ & \text{or } r'_{mI} \geq 6d, \\ 0 & \text{if } -6d \leq r'_{mI} < -2d \text{ or } 2d \leq r'_{mI} < 6d. \end{cases} \tag{28}$$

For the Q channel, the decision rules for bit q_1 and q_2 are given as displayed in Fig. 5 as

$$q_1 = \begin{cases} 1 & \text{if } r'_{mQ} < 0, \\ 0 & \text{if } r'_{mQ} \geq 0, \end{cases} \tag{29}$$

and

$$q_2 = \begin{cases} 1 & \text{if } r'_{mQ} < -2d \text{ or } r'_{mQ} \geq 2d, \\ 0 & \text{if } -2d \leq r'_{mQ} < 2d. \end{cases} \tag{30}$$

For a general decision rule of an arbitrary M_I-ary PAM with $\log_2 M_I$ being an integer, denote i_k as the symbol's $k-$th most significant bit ($k \leq \log_2 M_I$). As can be deduced from the two specific cases of 4-PAM and 8-PAM, a decision rule for i_k is given in the following form

$$i_k = \begin{cases} 1 & \text{if } r'_I \odot \mathcal{R}^{(1)}_{I_{M_I},k}, \\ 0 & \text{if } r'_I \odot \mathcal{R}^{(0)}_{I_{M_I},k}, \end{cases} \tag{31}$$

where $\mathcal{R}^{(1)}_{I_{M_I},k} = \left\{ \left(a^{(1)}_{I_{M_I},k} d, b^{(1)}_{I_{M_I},k} d \right) \middle| a^{(1)}_{I_{M_I},k} \in \{\mathbb{Z}, -\infty\}, b^{(1)}_{I_{M_I},k} \in \{\mathbb{Z}, +\infty\} \right\}$ and $\mathcal{R}^{(0)}_{I_{M_I},k} = \left\{ \left(a^{(0)}_{I_{M_I},k} d, b^{(0)}_{I_{M_I},k} d \right) \middle| a^{(0)}_{M_I,k} \in \mathbb{Z}, b^{(0)}_{M_I,k} \in \mathbb{Z} \right\}$ are the sets of decision regions of bits '1' and '0', respectively. In the above defined decision rule, we use the notation $r'_I \odot \mathcal{R}^{(1)}_{I_{M_I},k}$ (or $r'_I \odot \mathcal{R}^{(0)}_{I_{M_I},k}$) to imply that $a^{(1)}_{I_{M_I},k} d \leq r'_I < b^{(1)}_{I_{M_I},k} d$ for some $a^{(1)}_{I_{M_I},k} d$ and $b^{(1)}_{I_{M_I},k} d$ that $\left(a^{(1)}_{I_{M_I},k} d, b^{(1)}_{I_{M_I},k} d \right) \in \mathcal{R}^{(1)}_{I_{M_I},k}$. Note that $\mathcal{R}^{(0)}_{I_{M_I},k}$ and $\mathcal{R}^{(1)}_{I_{M_I},k}$ are disjoint. Next, let $\mathcal{A}^{(1)}_{I_{M_I},k} = \left\{ A^{(1)}_{I_{M_I},k} d \mid A^{(1)}_{I_{M_I},k} \in \mathbb{Z} \right\}$ and $\mathcal{A}^{(0)}_{I_{M_I},k} = \left\{ A^{(0)}_{I_{M_I},k} d \mid A^{(0)}_{I_{M_I},k} \in \mathbb{Z} \right\}$ be the sets of amplitudes of the original symbols whose i_k bits are '1' and '0', respectively. With these definitions, the conditional BER of i_k is given in (32), as shown at the bottom of the next page, where erfc(·) is the complementary error function. Similarly, with the same definitions for the Q channel, the conditional BER of q_k can be expressed in (33), as shown at the bottom of the next page.

The ABER is then given by

$$P_e = \int_0^{\infty} \int_{-\pi}^{\pi} P_{I,e}(i_k|\gamma_b, \theta_e) f_{\gamma_b}(\gamma_b) f_{\theta_e}(\theta_e) \, \mathrm{d}\theta_e \mathrm{d}\gamma_b + \int_0^{\infty} \int_{-\pi}^{\pi} P_{Q,e}(q_k|\gamma_b, \theta_e) f_{\gamma_b}(\gamma_b) f_{\theta_e}(\theta_e) \, \mathrm{d}\theta_e \mathrm{d}\gamma_b. \tag{34}$$

Though the expressions of $P_{I,e}(i_k|\gamma_b,\theta_e)$ and $P_{Q,e}(q_k|\gamma_b,\theta_e)$ are tedious, we observe that their summands are in the form $\text{erfc}\left(\frac{d}{\sqrt{2\sigma_n^2}}(\varphi+\psi\cos(\theta_e)+\omega\sin(\theta_e))\right)$ for some φ, ψ, and ω. As a result, it suffices to evaluate the following integral

$$P_e(\varphi,\psi,\omega)=\int_0^{\infty}\int_{-\pi}^{\pi}\text{erfc}\left(\frac{d}{\sqrt{2\sigma_n^2}}(\varphi+\psi\cos(\theta_e)+\omega\sin(\theta_e))\right)\times f_{\gamma_b}(\gamma_b)f_{\theta_e|\gamma_b}(\theta_e|\gamma_b)\,\mathrm{d}\theta_e\mathrm{d}\gamma_b. \quad (35)$$

$$\begin{aligned}
&P_{I,e}(i_k|\gamma_b,\theta_e)\\
&=\Pr\left(r_I'\odot\mathcal{R}_{I_{M_I,k}}^{(1)}\middle|r_I\in\mathcal{A}_{I_{M_I,k}}^{(0)}\right)+\Pr\left(r_I'\odot\mathcal{R}_{I_{M_I,k}}^{(0)}\middle|r_I\in\mathcal{A}_{I_{M_I,k}}^{(1)}\right)\\
&=\frac{1}{\log_2(M)M_IM_Q}\left(\sum_{r_I\in\mathcal{A}_{I_{M_I,k}}^{(0)}}\Pr\left(r_I'\odot\mathcal{R}_{I_{M_I,k}}^{(1)}\right)+\sum_{r_I\in\mathcal{A}_{I_{M_I,k}}^{(1)}}\Pr\left(r_I'\odot\mathcal{R}_{I_{M_I,k}}^{(0)}\right)\right)\\
&=\frac{1}{\log_2(M)M_IM_Q}\left(\sum_{A_{I_{M_I,k}}^{(0)}d\in\mathcal{A}_{I_{M_I,k}}^{(0)}}\sum_{\left(a_{I_{M_I,k}}^{(1)}d,b_{I_{M_I,k}}^{(1)}d\right)\in\mathcal{R}_{I_{M_I,k}}^{(1)}}\sum_{q=-\frac{M_Q}{2}}^{\frac{M_Q}{2}-1}\Pr\left(a_{I_{M_I,k}}^{(1)}d\le A_{I_{M_I,k}}^{(0)}d\cos(\theta_e)-(2q+1)d\sin(\theta_e)+n<b_{I_{M_I,k}}^{(1)}d\right)\right.\\
&\quad\left.+\sum_{A_{I_{M_I,k}}^{(1)}d\in\mathcal{A}_{I_{M_I,k}}^{(1)}}\sum_{\left(a_{I_{M_I,k}}^{(0)}d,b_{I_{M_I,k}}^{(0)}d\right)\in\mathcal{R}_{I_{M_I,k}}^{(0)}}\sum_{q=-\frac{M_Q}{2}}^{\frac{M_Q}{2}-1}\Pr\left(a_{I_{M_I,k}}^{(0)}d\le A_{I_{M_I,k}}^{(1)}d\cos(\theta_e)-(2q+1)d\sin(\theta_e)+n<b_{I_{M_I,k}}^{(0)}d\right)\right)\\
&=\frac{1}{2\log_2(M)M_IM_Q}\left(\sum_{A_{I_{M_I,k}}^{(0)}d\in\mathcal{A}_{I_{M_I,k}}^{(0)}}\sum_{\left(a_{I_{M_I,k}}^{(1)}d,b_{I_{M_I,k}}^{(1)}d\right)\in\mathcal{R}_{I_{M_I,k}}^{(1)}}\sum_{q=-\frac{M_Q}{2}}^{\frac{M_Q}{2}-1}\text{erfc}\left(\frac{a_{I_{M_I,k}}^{(1)}d-A_{I_{M_I,k}}^{(0)}d\cos(\theta_e)+(2q+1)d\sin(\theta_e)}{\sqrt{2\sigma_n^2}}\right)\right.\\
&\quad-\text{erfc}\left(\frac{b_{I_{M_I,k}}^{(1)}d-A_{I_{M_I,k}}^{(0)}d\cos(\theta_e)+(2q+1)d\sin(\theta_e)}{\sqrt{2\sigma_n^2}}\right)+\sum_{A_{I_{M_I,k}}^{(1)}d\in\mathcal{A}_{I_{M_I,k}}^{(1)}}\sum_{\left(a_{I_{M_I,k}}^{(0)}d,b_{I_{M_I,k}}^{(0)}d\right)\in\mathcal{R}_{I_{M_I,k}}^{(0)}}\sum_{q=-\frac{M_Q}{2}}^{\frac{M_Q}{2}-1}\\
&\quad\left.\times\text{erfc}\left(\frac{a_{I_{M_I,k}}^{(0)}d-A_{I_{M_I,k}}^{(1)}d\cos(\theta_e)+(2q+1)d\sin(\theta_e)}{\sqrt{2\sigma_n^2}}\right)-\text{erfc}\left(\frac{b_{I_{M_I,k}}^{(0)}d-A_{I_{M_I,k}}^{(1)}d\cos(\theta_e)+(2q+1)d\sin(\theta_e)}{\sqrt{2\sigma_n^2}}\right)\right). \quad (32)
\end{aligned}$$

$$\begin{aligned}
&P_{Q,e}(q_k|\gamma_b,\theta_e)\\
&=\frac{1}{2\log_2(M)M_IM_Q}\left(\sum_{A_{Q_{M_Q,k}}^{(0)}d\in\mathcal{A}_{Q_{M_Q,k}}^{(0)}}\sum_{\left(a_{Q_{M_Q,k}}^{(1)}d,b_{Q_{M_Q,k}}^{(1)}d\right)\in\mathcal{R}_{Q_{M_Q,k}}^{(1)}}\sum_{i=-\frac{M_I}{2}}^{\frac{M_I}{2}-1}\text{erfc}\left(\frac{a_{Q_{M_Q,k}}^{(1)}d-A_{Q_{M_Q,k}}^{(0)}d\cos(\theta_e)+(2i+1)d\sin(\theta_e)}{\sqrt{2\sigma_n^2}}\right)\right.\\
&\quad-\text{erfc}\left(\frac{b_{I_{M_I,k}}^{(1)}d-A_{I_{M_I,k}}^{(0)}d\cos(\theta_e)+(2i+1)d\sin(\theta_e)}{\sqrt{2\sigma_n^2}}\right)+\sum_{A_{Q_{M_Q,k}}^{(1)}d\in\mathcal{A}_{Q_{M_Q,k}}^{(1)}}\sum_{\left(a_{Q_{M_Q,k}}^{(0)}d,b_{Q_{M_Q,k}}^{(0)}d\right)\in\mathcal{R}_{Q_{M_Q,k}}^{(0)}}\sum_{q=-\frac{M_I}{2}}^{\frac{M_I}{2}-1}\\
&\quad\left.\times\text{erfc}\left(\frac{a_{Q_{M_Q,k}}^{(0)}d-A_{Q_{M_Q,k}}^{(1)}d\cos(\theta_e)+(2i+1)d\sin(\theta_e)}{\sqrt{2\sigma_n^2}}\right)-\text{erfc}\left(\frac{b_{Q_{M_Q,k}}^{(0)}d-A_{Q_{M_Q,k}}^{(1)}d\cos(\theta_e)+(2i+1)d\sin(\theta_e)}{\sqrt{2\sigma_n^2}}\right)\right).
\end{aligned} \quad (33)$$

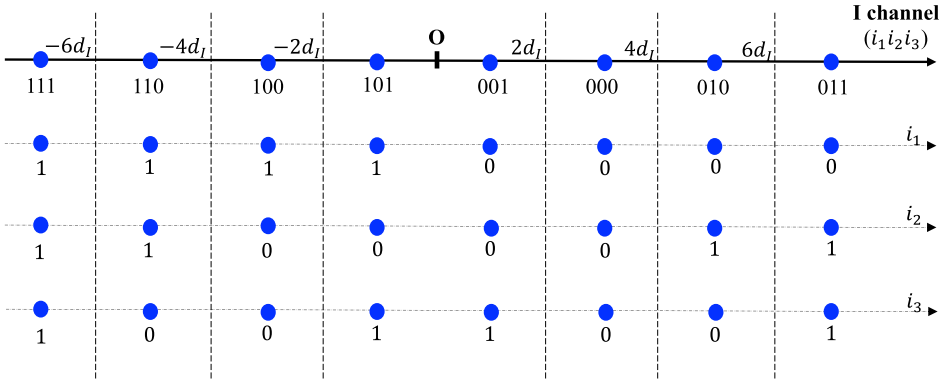

FIGURE 4. Bit-by-bit demapping on the I channel of the 8 × 4 QAM scheme.

Finding an exact closed-form solution to the above integral is general difficult (if not possible). To overcome this, our approach is to make use of a series of approximations. Firstly, in practice, the phase error value is usually very small (i.e. $\theta_e \approx 0$) resulting in $\cos(\theta_e) \approx 1$ and $\sin(\theta_e) \approx \theta$. Then, (35) is approximated by

$$P_e(\chi,\omega) \approx \int_0^{\infty}\int_{-\pi}^{\pi} \operatorname{erfc}\left(\frac{d}{\sqrt{2\sigma_n^2}}(\chi+\omega\theta_e)\right) \times f_{\gamma_b}(\gamma_b) f_{\theta_e|\gamma_b}(\theta_e|\gamma_b)\,\mathrm{d}\theta_e \mathrm{d}\gamma_b, \quad (36)$$

where $\chi = \varphi + \psi$. Moreover, at the higher value of PLL's SNR (i.e. $\rho \gg 1$), the Tikhonov distribution can be well approximated by the normal distribution (as shown in [36]) with zero-mean and variance $\frac{1}{C\gamma_b}$. Hence, the PDF of the turbulence-induced phase error can be rewritten following the normal distribution as

$$f_{\theta_e|\gamma_b}(\theta_e|\gamma_b) \approx \sqrt{\frac{C\gamma_b}{2\pi}} \exp\left(-\frac{\theta_e^2 C\gamma_b}{2}\right), \quad (37)$$

Using the well-known approximation $\operatorname{erfc}(x) \approx \frac{1}{6}\exp\left(-x^2\right) + \frac{1}{2}\exp\left(-\frac{4}{3}x^2\right)$, we now evaluate the inner integral in (36) as

$$\begin{aligned} P_e^{\text{inner}}(\chi,\omega) &= \int_{-\pi}^{\pi} \operatorname{erfc}\left(\frac{d}{\sqrt{2\sigma_n^2}}(\chi+\omega\theta_e)\right)\sqrt{\frac{C\gamma_b}{2\pi}}\exp\left(-\frac{\theta_e^2 C\gamma_b}{2}\right)\mathrm{d}\theta_e \\ &\approx \underbrace{\frac{1}{6}\int_{-\pi}^{\pi}\exp\left(-\frac{d^2}{2\sigma_n^2}(\chi+\omega\theta_e)^2\right)\sqrt{\frac{C\gamma_b}{2\pi}}\exp\left(-\frac{\theta_e^2 C\gamma_b}{2}\right)\mathrm{d}\theta_e}_{E(\chi,\omega)} \\ &\quad + \underbrace{\frac{1}{2}\int_{-\pi}^{\pi}\exp\left(-\frac{2d^2}{3\sigma_n^2}(\chi+\omega\theta_e)^2\right)\sqrt{\frac{C\gamma_b}{2\pi}}\exp\left(-\frac{\theta_e^2 C\gamma_b}{2}\right)\mathrm{d}\theta_e}_{F(\chi,\omega)}. \end{aligned} \quad (38)$$

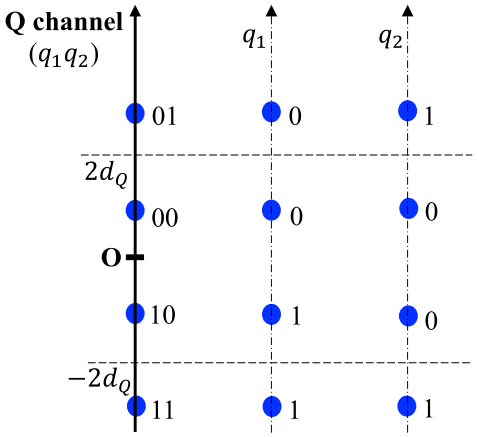

FIGURE 5. Bit-by-bit demapping on the Q channel of the 8 × 4 QAM scheme.

Closed-form expressions for $E(\chi,\omega)$ and $F(\chi,\omega)$ can be easily derived as

$$\begin{aligned} &E(\chi,\omega) \\ &= \frac{\sqrt{C}}{12\sqrt{2m}}\exp\left(\left(\frac{n^2}{4m}-u\right)\gamma_b\right) \\ &\quad\times\left(\operatorname{erf}\left(\frac{-2\pi m-n}{2\sqrt{m}}\sqrt{\gamma_b}\right)+\operatorname{erf}\left(\frac{-2\pi m+n}{2\sqrt{m}}\sqrt{\gamma_b}\right)\right), \end{aligned} \quad (39)$$

and

$$\begin{aligned} &F(\chi,\omega) \\ &= \frac{\sqrt{C}}{4\sqrt{2v}}\exp\left(\left(\frac{t^2}{4v}-p\right)\gamma_b\right) \\ &\quad\times\left(\operatorname{erf}\left(\frac{-2\pi v-t}{2\sqrt{v}}\sqrt{\gamma_b}\right)+\operatorname{erf}\left(\frac{-2\pi v+t}{2\sqrt{v}}\sqrt{\gamma_b}\right)\right), \end{aligned} \quad (40)$$

where $m = \frac{\omega^2 d^2}{2\sigma_n^2} + \frac{C}{2}$, $n = \frac{-\chi\omega d^2}{\sigma_n^2}$, $u = \frac{\chi d^2}{2\sigma^2}$, $v = \frac{2\omega^2 d^2}{3\sigma_n^2} + \frac{C}{2}$, $t = \frac{-4\chi\omega d^2}{3\sigma_n^2}$, $p = \frac{2\chi d^2}{3\sigma_n^2}$, and $\operatorname{erf}(\cdot)$ denotes the error function.

This allows us to rewrite (36) as

$$P_e(\chi,\omega) \approx \underbrace{\int_0^\infty E(\chi,\omega) f_{\gamma_b}(\gamma_b)\,\mathrm{d}\gamma_b}_{H_1(\chi,\omega)} + \underbrace{\int_0^\infty F(\chi,\omega) f_{\gamma_b}(\gamma_b)\,\mathrm{d}\gamma_b}_{H_2(\chi,\omega)}. \tag{41}$$

In the following, closed-form expressions for (41) are derived in the case of log-normal and gamma-gamma turbulence models.

1) LOG-NORMAL TURBULENCE CHANNEL

To facilitate deriving closed-form expressions for $H_1(\chi,\omega)$ and $H_2(\chi,\omega)$, it is necessary to utilize the following asymptotic behavior at high SNR of the combined PDF in (15) as [41]

$$\lim_{\gamma_b\to\infty} f_{\gamma_b}(\gamma_b) = \frac{\xi^2}{2(A_0h_l)^{\xi^2}} \frac{\gamma_b^{\frac{\xi^2}{2}-1}}{\overline{\gamma}_b^{\frac{\xi^2}{2}}} \exp\left(2\sigma_s^2\xi^2\left(1+\xi^2\right)\right) + O\left(\gamma_b^{\xi^2-1}\right), \tag{43}$$

where $O\left(\gamma_b^{\xi^2-1}\right)$ denotes the higher order of $\gamma_b^{\xi^2-1}$, which can be eliminated to get a simple approximation of $f_{\gamma_b}(\gamma_b)$ with a satisfactory accuracy. Using this approximation, we get

$$\begin{aligned} H_1(\chi,\omega) &\approx \frac{\sqrt{C}}{12\sqrt{2m}} \frac{\xi^2}{2(A_0h_l)^{\xi^2}\overline{\gamma}_b^{\xi^2/2}} \exp\left(2\sigma_s^2\xi^2\left(1+\xi^2\right)\right) \\ &\times \int_0^\infty \gamma_b^{\frac{\xi^2}{2}-1} \exp\left(\left(\frac{n^2}{4m}-u\right)\gamma_b\right) \\ &\times \left(\mathrm{erf}\left(\frac{-2\pi m-n}{2\sqrt{m}}\sqrt{\gamma_b}\right)+\mathrm{erf}\left(\frac{-2\pi m+n}{2\sqrt{m}}\sqrt{\gamma_b}\right)\right)\mathrm{d}\gamma_b, \end{aligned} \tag{44}$$

and

$$\begin{aligned} H_2(\chi,\omega) &\approx \frac{\sqrt{C}}{4\sqrt{2v}} \frac{\xi^2}{2(A_0h_l)^{\xi^2}\overline{\gamma}_b^{\xi^2/2}} \exp\left(2\sigma_s^2\xi^2\left(1+\xi^2\right)\right) \\ &\times \int_0^\infty \gamma_b^{\frac{\xi^2}{2}-1} \exp\left(\left(\frac{t^2}{4v}-p\right)\gamma_b\right) \\ &\times \left(\mathrm{erf}\left(\frac{-2\pi v-t}{2\sqrt{v}}\sqrt{\gamma_b}\right)+\mathrm{erf}\left(\frac{-2\pi v+t}{2\sqrt{v}}\sqrt{\gamma_b}\right)\right)\mathrm{d}\gamma_b. \end{aligned} \tag{45}$$

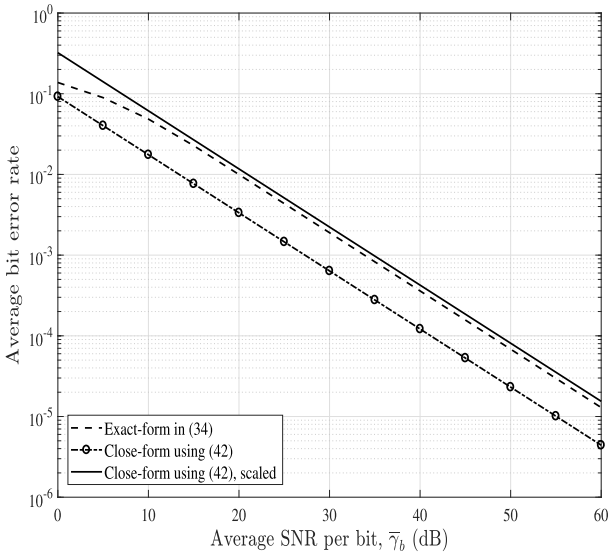

FIGURE 6. Exact, approximate, and adjusted ABERs in log-normal turbulence channel with $L = 1000$ m, $C_n^2 = 5 \times 10^{-15}$, and $C = 5$ dB.

Using the identity $\mathrm{erf}(x) = \frac{x}{\sqrt{\pi}} G_{1,2}^{1,1}\left(x^2 \middle| \begin{matrix} 1/2 \\ 0, -1/2 \end{matrix}\right)$ and [44, Eq. (2.24.3.1)], a closed-form expression for $P_e(\chi,\omega)$ in the case of log-normal turbulence channel is given in (42), as shown at the bottom of the page.

Fig. 6 shows the exact and approximate ABERs computed using (34) and (42) with $C_n^2 = 5 \times 10^{-15}$, FSO link distance of $L = 1000$ m, and $C = 5$ dB. Parameters related to pointing misalignment are chosen as $\xi = 1.2$ and $A_0 = 2$. It is observed that at $\overline{\gamma}_b \geq 10$ dB, the approximate ABER differs linearly from the exact one due to the use of several approximations. However, it is interesting that this linear discrepancy can be compensated by scaling the approximate BER by a factor of 3.5.

$$\begin{aligned} P_e^{\mathrm{LN}}(\chi,\omega) \approx{}& \frac{1}{\sqrt{\pi}} \frac{\xi^2\sqrt{C}}{2(A_0h_l)^{\xi^2}\overline{\gamma}_b^{\xi^2/2}} \exp\left(2\sigma_s^2\xi^2\left(1+\xi^2\right)\right) \\ &\times \left\{ \frac{\left(u-\frac{n^2}{4m}\right)^{-\frac{\xi^2}{2}}}{12\sqrt{2m}} \left(G_{2,2}^{1,2}\left[\frac{(2\pi m+n)^2}{4mu-n^2}\middle| \begin{matrix} 1-\frac{\xi^2}{2}, 1 \\ \frac{1}{2}, 0 \end{matrix}\right] + G_{2,2}^{1,2}\left[\frac{(-2\pi m+n)^2}{4mu-n^2}\middle| \begin{matrix} 1-\frac{\xi^2}{2}, 1 \\ \frac{1}{2}, 0 \end{matrix}\right]\right) \right. \\ &\left. + \frac{\left(p-\frac{t^2}{4v}\right)^{-\frac{\xi^2}{2}}}{4\sqrt{2m}} \left(G_{2,2}^{1,2}\left[\frac{(2\pi v+t)^2}{4vp-t^2}\middle| \begin{matrix} 1-\frac{\xi^2}{2}, 1 \\ \frac{1}{2}, 0 \end{matrix}\right] + G_{2,2}^{1,2}\left[\frac{(-2\pi v+t)^2}{4vp-t^2}\middle| \begin{matrix} 1-\frac{\xi^2}{2}, 1 \\ \frac{1}{2}, 0 \end{matrix}\right]\right) \right\}. \end{aligned} \tag{42}$$

2) GAMMA-GAMMA TURBULENCE CHANNEL

For the moderate to strong turbulence, the gamma-gamma distribution is used to model the turbulence channel. Then, the closed-form of Eq. (34) is obtained following another way. By substituting Eq. (20) and Eq. (40) into Eq. (41), the integral H_1 can be shown as

$$H_1(\chi,\omega) = \int_0^\infty \frac{\sqrt{C}}{24\sqrt{2m}} \exp\left[\left(\frac{n^2}{4m}-u\right)\gamma_b\right] \times \left[\mathrm{erf}\left(\frac{-2\pi m-n}{2\sqrt{m}}\sqrt{\gamma_b}\right) + \mathrm{erf}\left(\frac{-2\pi m+n}{2\sqrt{m}}\sqrt{\gamma_b}\right)\right] \times G_{1,3}^{3,0}\left[\frac{\alpha\beta\xi^2}{(\xi^2+1)}\sqrt{\frac{\gamma_b}{\overline{\gamma}_b}}\,\middle|\,\begin{matrix}\Psi(\xi)\\ \Delta(\xi,\alpha,\beta)\end{matrix}\right] \mathrm{d}\gamma_b, \quad (47)$$

and

$$H_2(\chi,\omega) = \int_0^\infty \frac{\sqrt{C}}{8\sqrt{2v}} \exp\left[\left(\frac{t^2}{4v}-p\right)\gamma_b\right] \times \left[\mathrm{erf}\left(\frac{-2\pi v-t}{2\sqrt{v}}\sqrt{\gamma_b}\right) + \mathrm{erf}\left(\frac{-2\pi v+t}{2\sqrt{v}}\sqrt{\gamma_b}\right)\right] \times G_{1,3}^{3,0}\left[\frac{\alpha\beta\xi^2}{(\xi^2+1)}\sqrt{\frac{\gamma_b}{\overline{\gamma}_b}}\,\middle|\,\begin{matrix}\Psi(\xi)\\ \Delta(\xi,\alpha,\beta)\end{matrix}\right] \mathrm{d}\gamma_b, \quad (48)$$

where $\Psi(\xi) = \left\{1, \frac{\xi^2+1}{2}, \frac{\xi^2}{2}+1\right\}$, $\Delta(\xi,\alpha,\beta) = \left\{\frac{\xi^2}{2}, \frac{\xi^2+1}{2}, \frac{\alpha}{2}, \frac{\alpha+1}{2}, \frac{\beta}{2}, \frac{\beta+1}{2}\right\}$. Finally, by using $\mathrm{erf}(x) = 1-\mathrm{erfc}(x)$, $\mathrm{erfc}(x) \approx \frac{1}{6}\exp\left(-x^2\right)+\frac{1}{2}\exp\left(-\frac{4}{3}x^2\right)$, ([44], Eq. (2.24.3.1)), and denoting $W = \frac{\alpha\beta\xi^2}{(\xi^2+1)\sqrt{\overline{\gamma}_b}}$, $R = u-\frac{n^2}{4m}$, and $Y = p-\frac{t^2}{4v}$, a closed-form expression for the ABER in this case is given in (46), as shown at the bottom of the page.

In this case, we also observe linear discrepancies between the exact and approximate ABERs as illustrated in Fig. 7 with different values of C_n^2. However, the scaling factor is shown to be 1.5.

IV. NUMERICAL RESULTS

In this section, representative numerical results are presented to illustrate the BER performances of SIM-QAM FSO systems under the impacts of atmospheric turbulence and phase error. To verify the accuracy of the analytical derivations, Monte-Carlo simulations are performed. Without otherwise noted, the fraction of collected power at $L = 0$, $A_0 = 2$, the radius of the photodetector aperture, $a = 0.1$ m, the beam waist radius at $L = 0$, $w_0 = 0.05$ m, and the optical wavelength, $\lambda = 1550$ nm are chosen.

A. PERFORMANCES WITHOUT POINTING MISALIGNMENT

Firstly, we show the ABER performances assuming a perfect pointing alignment. In the case of weak turbulence modeled by log-normal distribution with $C_n^2 = 10^{-15}$, Fig. 8 compares performances of different QAM constellation sizes (e.g. 4×4 and 8×4 QAM) for different values of the average SNR per bit where the link length is set to 1000 m. As shown in (22), the phase error distribution is solely scaled by the constant

$$P_e^{\mathrm{GG}}(\chi,\omega) \approx \frac{\sqrt{C}}{96\pi\sqrt{2m}} \frac{2^{\alpha+\beta-1}\xi^2}{\Gamma(\alpha)\Gamma(\beta)} \left\{ 2G_{3,6}^{6,1}\left[\frac{W^2}{16R}\,\middle|\,\begin{matrix}\Psi(\xi)\\ \Delta(\xi,\alpha,\beta)\end{matrix}\right] - \frac{1}{6}G_{3,6}^{6,1}\left[\frac{W^2}{16\left(\left(\frac{2\pi m+n}{2\sqrt{m}}\right)^2+R\right)}\,\middle|\,\begin{matrix}\Psi(\xi)\\ \Delta(\xi,\alpha,\beta)\end{matrix}\right] - \frac{1}{2}G_{3,6}^{6,1}\left[\frac{W^2}{16\left(\frac{4}{3}\left(\frac{2\pi m+n}{2\sqrt{m}}\right)^2+R\right)}\,\middle|\,\begin{matrix}\Psi(\xi)\\ \Delta(\xi,\alpha,\beta)\end{matrix}\right] - \frac{1}{6}G_{3,6}^{6,1}\left[\frac{W^2}{16\left(\left(\frac{-2\pi m+n}{2\sqrt{m}}\right)^2+R\right)}\,\middle|\,\begin{matrix}\Psi(\xi)\\ \Delta(\xi,\alpha,\beta)\end{matrix}\right] - \frac{1}{2}G_{3,6}^{6,1}\left[\frac{W^2}{16\left(\frac{4}{3}\left(\frac{-2\pi m+n}{2\sqrt{m}}\right)^2+R\right)}\,\middle|\,\begin{matrix}\Psi(\xi)\\ \Delta(\xi,\alpha,\beta)\end{matrix}\right] \right\} + \frac{\sqrt{C}}{32\pi\sqrt{2v}} \frac{2^{\alpha+\beta-1}\xi^2}{\Gamma(\alpha)\Gamma(\beta)} \left\{ 2G_{3,6}^{6,1}\left[\frac{W^2}{16Y}\,\middle|\,\begin{matrix}\Psi(\xi)\\ \Delta(\xi,\alpha,\beta)\end{matrix}\right] - \frac{1}{6}G_{3,6}^{6,1}\left[\frac{W^2}{16\left(\left(\frac{2\pi v+t}{2\sqrt{v}}\right)^2+Y\right)}\,\middle|\,\begin{matrix}\Psi(\xi)\\ \Delta(\xi,\alpha,\beta)\end{matrix}\right] - \frac{1}{2}G_{3,6}^{6,1}\left[\frac{W^2}{16\left(\frac{4}{3}\left(\frac{2\pi v+t}{2\sqrt{v}}\right)^2+Y\right)}\,\middle|\,\begin{matrix}\Psi(\xi)\\ \Delta(\xi,\alpha,\beta)\end{matrix}\right] - \frac{1}{6}G_{3,6}^{6,1}\left[\frac{W^2}{16\left(\left(\frac{-2\pi v+t}{2\sqrt{v}}\right)^2+Y\right)}\,\middle|\,\begin{matrix}\Psi(\xi)\\ \Delta(\xi,\alpha,\beta)\end{matrix}\right] - \frac{1}{2}G_{3,6}^{6,1}\left[\frac{W^2}{16\left(\frac{4}{3}\left(\frac{-2\pi v+t}{2\sqrt{v}}\right)^2+Y\right)}\,\middle|\,\begin{matrix}\Psi(\xi)\\ \Delta(\xi,\alpha,\beta)\end{matrix}\right] \right\}. \quad (46)$$

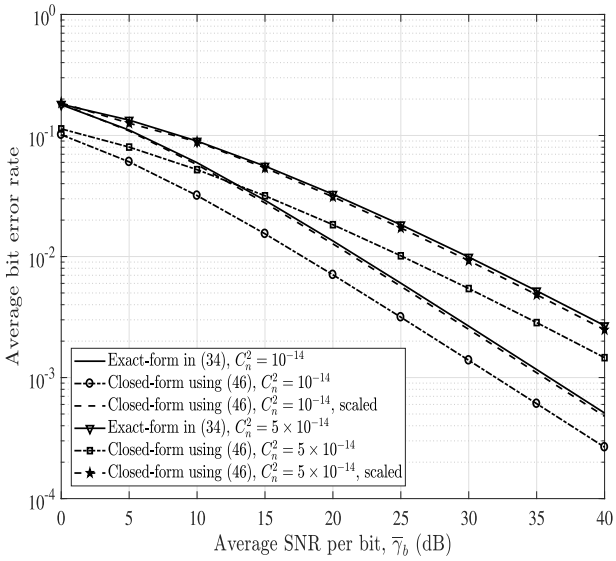

FIGURE 7. Exact, approximate, and adjusted ABERs in gamma-gamma turbulence channel with $L = 1000$ m and $C = 5$ dB.

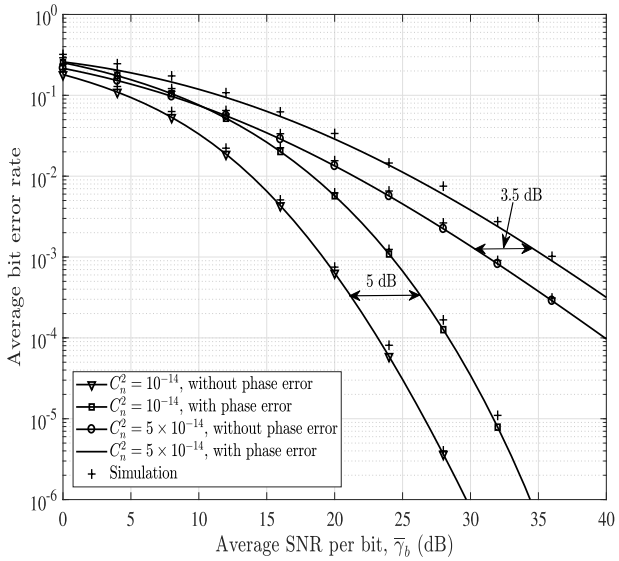

FIGURE 9. ABER versus average SNR per bit $\overline{\gamma}_b$ with $L = 1000$ m and $C = 5$.

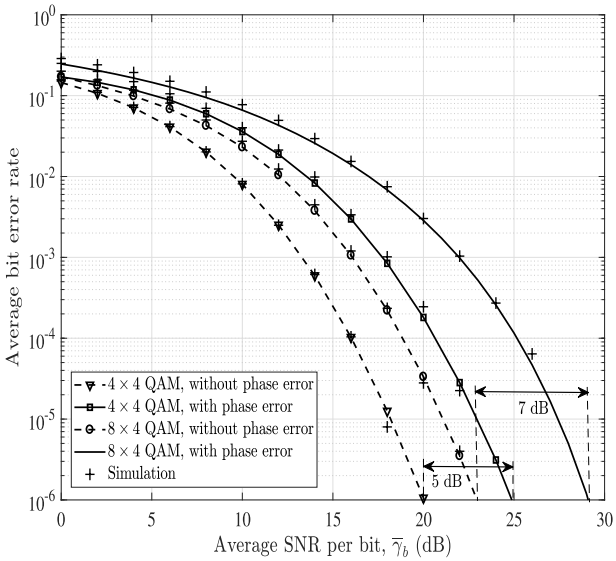

FIGURE 8. ABER versus average SNR per bit $\overline{\gamma}_b$ in weak turbulence with $C_n^2 = 5 \times 10^{-15}$, $L = 1000$ m, $C = 5$.

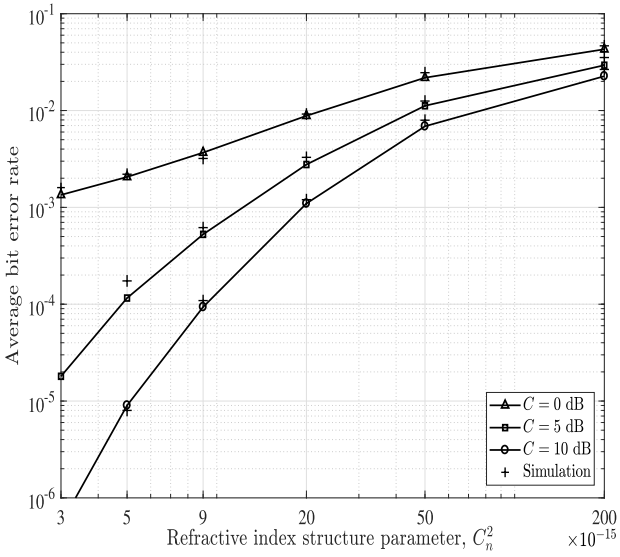

FIGURE 10. ABER versus C_n^2 for different values of C with $\overline{\gamma}_b = 25$ dB, and $L = 1000$ m.

factor C, which is set to 5 in this case. We can observe a significant adverse impact of phase error as compared to the 8×4 QAM without phase error, the 4×4 with phase error suffers higher ABER. Similar to PSK, it is evident that the performance loss due to phase error increases proportionally in accordance with an increase in the modulation order. For example, the phase error results in 5 and 7 dB power losses in the case of 4×4 and 8×4 QAM, respectively. This emphasizes the potential severity of phase error since practical systems usually employ high order QAM modulation for applications requiring high data-rates.

ABER performances are displayed in Fig. 9 in moderate (i.e. $C_n^2 = 10^{-14}$) and strong (i.e. $C_n^2 = 5 \times 10^{-14}$) turbulence regimes, which are modeled by the gamma-gamma distribution. Similar to the case of modulation order, the impact of phase error on ABER varies with respect to the turbulence strength. Qualitatively, the weaker the turbulence is, the greater performance loss due phase error becomes.

The advantage of using PLL to alleviate the influence of turbulence-induced phase error is shown in Fig. 10. The average SNR per bit $\overline{\gamma}_b$ is chosen to be 25 dB. There difference values of C, namely 0, 5, and 10 dB are examined over a wide range of turbulence strength (i.e. C_n^2 varies from 3×10^{-15} to 2×10^{-13}). On the one hand, it is obvious that the system performance improves as C increases. This is also a result of the fact that the phase error variance is inversely proportional to C. On the other hand, the performance gain benefited from

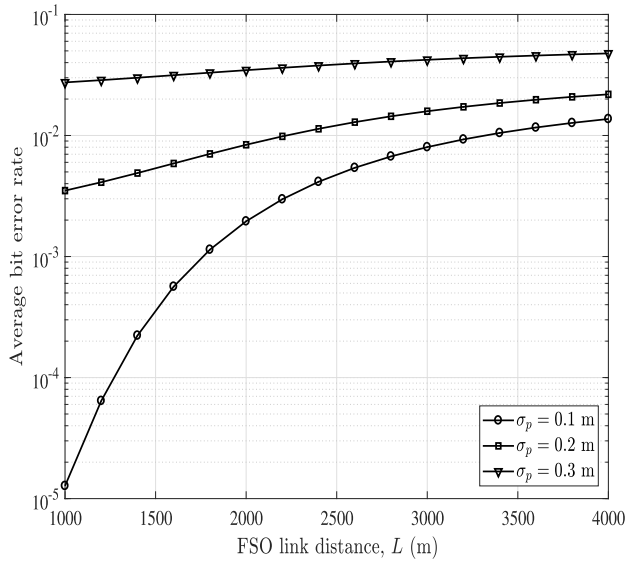

FIGURE 11. ABER versus link distance L with $C_n^2 = 10^{-14}$, $\overline{\gamma}_b = 20$ dB, $C = 5$ dB.

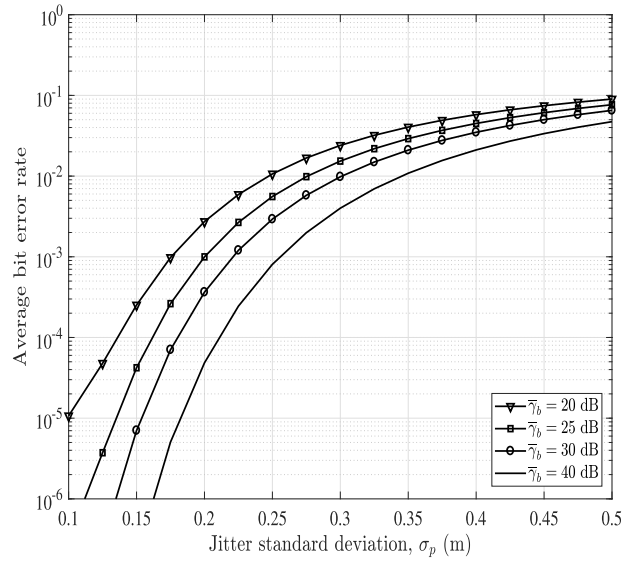

FIGURE 12. ABER versus jitter standard deviation σ_p with $C_n^2 = 10^{-14}$, $L = 1000$ m, $C = 5$ dB.

increasing C vanishes when the turbulence gets stronger. For instance, by increasing C from 0 to 10 dB, the ABER reduces from 8×10^{-2} to 10^{-5} when $C_n^2 = 5 \times 10^{-15}$ (i.e. weak turbulence) while the reduction is from 10^{-2} to 10^{-3} when $C_n^2 = 5 \times 10^{-14}$ (i.e. strong turbulence). Hence, one should employ PLL with high values of C in the case of weak turbulence conditions.

B. PERFORMANCES WITH POINTING MISALIGNMENT

We now present numerical results in the case with the presence of pointing misalignment. The relationship between ABER and the link distance L is considered for different values of the jitter standard deviation in Fig. 11 with $C_n^2 = 10^{-14}$, $\overline{\gamma}_b = 20$ dB, $C = 5$ dB, and receiver radius $a = 0.1$ m. It is seen that a standard deviation $\sigma_p \geq 0.2$ m renders the system dysfunctional (i.e. ABER $\geq 10^{-3}$) regardless of the typical transmission distance (i.e. $L \geq 1000$ m). The performance loss resulted from misalignment is particularly significant at short link distances due to small beam footprints. As the size of the beam footprint increases when L increases, the system is more resilient to misalignment. In this scenario, the system performance is degraded mainly due to geometric loss and turbulence-induced fading. The severity of pointing misalignment is again illustrated in Fig. 12, where various values of average SNR per bit $\overline{\gamma}_b$ are considered. We observe that even with $\overline{\gamma}_b$ as high as 40 dB, the system suffers from high ABER ($\geq 10^{-5}$) when $\sigma_p \geq 0.2$ m. Together with the previous results, a jitter standard deviation of less than 0.2 m is required for the system operating reliably.

V. CONCLUSION

The impact of the pointing misalignment, turbulence-induced fading, and phase error on the ABER of SIM-QAM FSO systems is studied in this article. The Tikhonov distribution is used to model phase error while the turbulence-induced fading is described by log-normal distribution (in the weak turbulence regime) and gamma-gamma distribution (in the moderate and strong turbulence regimes). Numerical results showed that the effect of turbulence-induced phase error on the performance is severe especially in weak turbulence and high order modulation (i.e. large constellation sizes) while fading is the dominant factor in the moderate-to-strong turbulence regime. The system performance loss due to turbulence-induced atmospheric turbulence can be effectively improved by utilizing PLL. In addition to the phase error, the pointing misalignment is shown to be a significant performance-degrading factor.

REFERENCES

[1] D. Jokanovic and M. Josipovic, "RF spectrum congestion: Resolving an interference case," in *Proc. IEEE Int. Conf. Microw., Commun., Antennas Electron. Syst. (COMCAS)*, Nov. 2011, pp. 1–4.
[2] H. A. Willebrand and B. S. Ghuman, *Free Space Optics: Enabling Optical Connectivity in Today's Networks*. Indianapolis, IN, USA: SAMS, 2002.
[3] V. W. S. Chan, "Free-space optical communications," *J. Lightw. Technol.*, vol. 24, no. 12, pp. 4750–4762, Dec. 2006.
[4] W. P. Z. Ghassemlooy and S. Rajbhandari, *Optical Wireless Communications: System and Channel Modelling With MATLAB*. Abingdon, U.K.: Taylor & Francis, 2013.
[5] M. A. Khalighi and M. Uysal, "Survey on free space optical communication: A communication theory perspective," *IEEE Commun. Surveys Tuts.*, vol. 16, no. 4, pp. 2231–2258, Jun. 2014.
[6] M. Safari and M. Uysal, "Relay-assisted free-space optical communication," *IEEE Trans. Wireless Commun.*, vol. 7, no. 12, pp. 5441–5449, Dec. 2008.
[7] C. Abou-Rjeily, "Performance analysis of FSO communications with diversity methods: Add more relays or more apertures?" *IEEE J. Sel. Areas Commun.*, vol. 33, no. 9, pp. 1890–1902, Sep. 2015.
[8] T. V. Pham, T. C. Thang, and A. T. Pham, "Average achievable rate of spatial diversity MIMO-FSO over correlated Gamma–Gamma fading channels," *IEEE/OSA J. Opt. Commun. Netw.*, vol. 10, no. 8, pp. 662–674, Aug. 2018.
[9] A. Jaiswal, M. Abaza, M. R. Bhatnagar, and V. K. Jain, "An investigation of performance and diversity property of optical space shift keying-based FSO-MIMO system," *IEEE Trans. Commun.*, vol. 66, no. 9, pp. 4028–4042, Sep. 2018.

[10] K. Kiasaleh, "Performance of APD-based, PPM free-space optical communication systems in atmospheric turbulence," *IEEE Trans. Commun.*, vol. 53, no. 9, pp. 1455–1461, Sep. 2005.

[11] W. Gappmair, S. Hranilovic, and E. Leitgeb, "Performance of PPM on terrestrial FSO links with turbulence and pointing errors," *IEEE Commun. Lett.*, vol. 14, no. 5, pp. 468–470, May 2010.

[12] J. Li, J. Q. Liu, and D. P. Taylor, "Optical communication using subcarrier PSK intensity modulation through atmospheric turbulence channels," *IEEE Trans. Commun.*, vol. 55, no. 8, pp. 1598–1606, Aug. 2007.

[13] W. O. Popoola and Z. Ghassemlooy, "BPSK subcarrier intensity modulated free-space optical communications in atmospheric turbulence," *J. Lightw. Technol.*, vol. 27, no. 8, pp. 967–973, Apr. 2009.

[14] H. Samimi, "Optical communication using subcarrier intensity modulation through generalized turbulence channels," *IEEE/OSA J. Opt. Commun. Netw.*, vol. 4, no. 5, pp. 378–381, May 2012.

[15] D. A. Luong, A. T. Pham, and T. C. Thang, "Effect of avalanche photodiode and thermal noises on the performance of binary phase-shift keying-subcarrier-intensity modulation/free-space optical systems over turbulence channels," *IET Commun.*, vol. 7, no. 8, pp. 738–744, May 2013.

[16] T. V. Pham and A. T. Pham, "Performance analysis of amplify–decode-and-forward multihop binary phase-shift keying/free-space optical systems using avalanche photodiode receivers over atmospheric turbulence channels," *IET Commun.*, vol. 8, no. 9, pp. 1518–1526, Jun. 2014.

[17] M. R. Bhatnagar and Z. Ghassemlooy, "Performance analysis of gamma–gamma fading FSO MIMO links with pointing errors," *J. Lightw. Technol.*, vol. 34, no. 9, pp. 2158–2169, 2016.

[18] J. R. Alexovich and R. M. Gagliardi, "The effect of phase noise on noncoherent digital communications," *IEEE Trans. Commun.*, vol. 38, no. 9, pp. 1539–1548, Sep. 1990.

[19] A. G. Burr, "Comparison of coherent and non coherent modulation in the presence of phase noise," *IEE Proc. I, Commun., Speech Vis.*, vol. 139, no. 2, pp. 147–155, Apr. 1992.

[20] X. Song, F. Yang, J. Cheng, N. Al-Dhahir, and Z. Xu, "Subcarrier phase-shift keying systems with phase errors in lognormal turbulence channels," *J. Lightw. Technol.*, vol. 33, no. 9, pp. 1896–1904, May 1, 2015.

[21] W. Gappmair and H. E. Nistazakis, "Subcarrier PSK performance in terrestrial FSO links impaired by gamma-gamma fading, pointing errors, and phase noise," *J. Lightw. Technol.*, vol. 35, no. 9, pp. 1624–1632, May 1, 2017.

[22] M. I. Petkovic, G. T. Djordjevic, G. K. Karagiannidis, and G. V. Milovanovic, "Performance of SIM-MDPSK FSO systems with hardware imperfections," *IEEE Trans. Wireless Commun.*, vol. 16, no. 8, pp. 5442–5451, Aug. 2017.

[23] G. K. Varotsos, H. E. Nistazakis, W. Gappmair, H. G. Sandalidis, and G. S. Tombras, "SIMO subcarrier PSK FSO links with phase noise and non-zero boresight pointing errors over turbulence channels," *IET Commun.*, vol. 13, no. 7, pp. 831–836, Apr. 2019.

[24] A. C. M. Lee and P. J. McLane, "Convolutionally interleaved PSK and DPSK trellis codes for shadowed, fast fading mobile satellite communication channels," *IEEE Trans. Veh. Technol.*, vol. 39, no. 1, pp. 37–47, Feb. 1990.

[25] P. Supnithi, W. Wongtrairat, and S. Tantaratana, "Performance of M-PSK in mobile satellite communication over combined ionospheric scintillation and flat fading channels with MRC diversity," *IEEE Trans. Wireless Commun.*, vol. 8, no. 7, pp. 3360–3364, Jul. 2009.

[26] P. K. Singya, N. Kumar, V. Bhatia, and M.-S. Alouini, "On the performance analysis of higher order QAM schemes over mixed RF/FSO systems," *IEEE Trans. Veh. Technol.*, vol. 69, no. 7, pp. 7366–7378, Jul. 2020.

[27] P. Yang, Y. Xiao, B. Zhang, S. Li, M. El-Hajjar, and L. Hanzo, "Star-QAM signaling constellations for spatial modulation," *IEEE Trans. Veh. Technol.*, vol. 63, no. 8, pp. 3741–3749, Oct. 2014.

[28] K. Ishibashi, W.-Y. Shin, H. Ochiai, and V. Tarokh, "A peak power efficient cooperative diversity using star-QAM with Coherent/Noncoherent detection," *IEEE Trans. Wireless Commun.*, vol. 12, no. 5, pp. 2137–2147, May 2013.

[29] X.-C. Zhang, H. Yu, and G. Wei, "Exact symbol error probability of cross-QAM in AWGN and fading channels," *EURASIP J. Wireless Commun. Netw.*, vol. 2010, no. 1, pp. 917–954, Dec. 2010.

[30] K. P. Peppas and C. K. Datsikas, "Average symbol error probability of general-order rectangular quadrature amplitude modulation of optical wireless communication systems over atmospheric turbulence channels," *IEEE/OSA J. Opt. Commun. Netw.*, vol. 2, no. 2, pp. 102–110, Feb. 2010.

[31] M. Zoheb Hassan, X. Song, and J. Cheng, "Subcarrier intensity modulated wireless optical communications with rectangular QAM," *IEEE/OSA J. Opt. Commun. Netw.*, vol. 4, no. 6, pp. 522–532, Jun. 2012.

[32] B. T. Vu, N. T. Dang, T. C. Thang, and A. T. Pham, "Bit error rate analysis of rectangular QAM/FSO systems using an APD receiver over atmospheric turbulence channels," *IEEE/OSA J. Opt. Commun. Netw.*, vol. 5, no. 5, pp. 437–446, May 2013.

[33] H. S. Khallaf, H. M. H. Shalaby, J. M. Garrido-Balsells, and S. Sampei, "Performance analysis of a hybrid QAM-MPPM technique over turbulence-free and gamma-gamma free-space optical channels," *IEEE/OSA J. Opt. Commun. Netw.*, vol. 9, no. 2, pp. 161–171, Feb. 2017.

[34] F. J. Escribano and A. Wagemakers, "Performance analysis of QAM-MPPM in turbulence-free FSO channels: Accurate derivations and practical approximations," *IEEE Syst. J.*, early access, May 12, 2020, doi: 10.1109/JSYST.2020.2986680.

[35] H. Singh and A. S. Sappal, "Analytic and simulative comparison of turbulent FSO system with different modulation techniques," *Opt. Laser Technol.*, vol. 114, pp. 49–59, Jun. 2019. [Online]. Available: http://www.sciencedirect.com/science/article/pii/S0030399218302299

[36] T. V. Nguyen, A.-T.-H. Bui, N. T. Dang, and A. T. Pham, "Performance of SIM/S-QAM FSO systems with phase errors in gamma-gamma turbulence channels," in *Proc. Int. Conf. Inf. Commun. Technol. Converg. (ICTC)*, Oct. 2018, pp. 85–90.

[37] A. A. Farid and S. Hranilovic, "Outage capacity optimization for free-space optical links with pointing errors," *J. Lightw. Technol.*, vol. 25, no. 7, pp. 1702–1710, Jul. 2007.

[38] D. K. Borah and D. G. Voelz, "Pointing error effects on free-space optical communication links in the presence of atmospheric turbulence," *J. Lightw. Technol.*, vol. 27, no. 18, pp. 3965–3973, Sep. 2009.

[39] K. Cho and D. Yoon, "On the general BER expression of one- and two-dimensional amplitude modulations," *IEEE Trans. Commun.*, vol. 50, no. 7, pp. 1074–1080, Jul. 2002.

[40] A. Mansour, R. Mesleh, and M. Abaza, "New challenges in wireless and free space optical communications," *Opt. Lasers Eng.*, vol. 89, pp. 95–108, Feb. 2017. [Online]. Available: http://www.sciencedirect.com/science/article/pii/S0143816616300252

[41] T. Ismail and E. Leitgeb, "Performance analysis of SIM-DPSK FSO system over lognormal fading with pointing errors," in *Proc. 18th Int. Conf. Transparent Opt. Netw. (ICTON)*, Jul. 2016, pp. 1–4.

[42] M. A. Al-Habash, L. C. Andrews, and R. L. Phillips, "Mathematical model for the irradiance probability density function of a laser beam propagating through turbulent media," *Opt. Eng.*, vol. 40, pp. 1554–1562, Aug. 2001. [Online]. Available: https://doi.org/10.1117/1.1386641

[43] G. T. Djordjevic, M. I. Petkovic, A. M. Cvetkovic, and G. K. Karagiannidis, "Mixed RF/FSO relaying with outdated channel state information," *IEEE J. Sel. Areas Commun.*, vol. 33, no. 9, pp. 1935–1948, Sep. 2015.

[44] A. Prudnikov, Y. Brychkov, and O. Marichev, *Integrals and Series, More Special Functions*, vol. 3. London, U.K.: Gordon and Breach Science, 1986.

[45] W. Weber, "Performance of phase-locked loops in the presence of fading communication channels," *IEEE Trans. Commun.*, vol. COM-24, no. 5, pp. 487–499, May 1976.

THANG V. NGUYEN (Graduate Student Member, IEEE) received the B.E. degree in electronics and telecommunications engineering from the Posts and Telecommunications Institute of Technology (PTIT), Vietnam, in 2017, and the M.E. degree in computer science and engineering from The University of Aizu (UoA), Japan, in 2019, where he is currently pursuing the Ph.D. degree in computer science and engineering. His current research interests include network modeling and performance analysis with a particular emphasis on optical wireless communications.

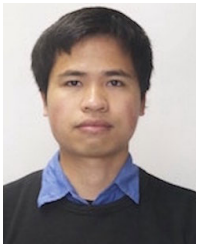

THANH V. PHAM (Member, IEEE) received the B.E., M.E., and Ph.D. degrees in computer science and engineering from The University of Aizu, Japan, in 2014, 2016, and 2019, respectively. He was a Japan Society for the Promotion of Science (JSPS) Doctoral and Postdoctoral Fellow, from 2018 to 2020. He is currently a special Postdoctoral Researcher with The University of Aizu. His research interests include free-space optics (FSO), relay networks, and visible light communications (VLC). He is a member of IEICE.

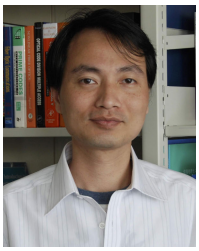

NGOC T. DANG (Member, IEEE) received the B.E. degree in electronics and telecommunications from the Hanoi University of Technology, Hanoi, Vietnam, in 1999, the M.E. degree in electronics and telecommunications from the Posts and Telecommunications Institute of Technology (PTIT), Hanoi, in 2005, and the Ph.D. degree in computer science and engineering from The University of Aizu, Aizuwakamatsu, Japan, in 2010. He is currently an Associate Professor/Head of the Department of Wireless Communications, PTIT. He was also an Invited/Visiting Researcher with the FOTON ENSSAT Laboratory, Universite de Rennes 1, France, in 2011, and the Computer Communications Laboratory, The University of Aizu, in 2012, 2013, 2015, and 2017. His current research interests include the area of communication theory with a particular emphasis on modeling, design, and performance evaluation of optical CDMA, RoF, optical wireless communication, and quantum key distribution systems.

ANH T. PHAM (Senior Member, IEEE) received the B.E. and M.E. degrees in electronics engineering from the Hanoi University of Technology, Vietnam, in 1997 and 2000, respectively, and the Ph.D. degree in information and mathematical sciences from Saitama University, Japan, in 2005. From 1998 to 2002, he was with NTT Corporation, Vietnam. Since 2005, he has been a Faculty Member with The University of Aizu, where he is currently a Professor and the Head of the Computer Communications Laboratory, Division of Computer Engineering. His research interests include the broad areas of communication theory and networking with a particular emphasis on modeling, design, and performance evaluation of wired/wireless communication systems and networks. He has authored/coauthored over 160 peer-reviewed articles on these topics. He is also a member of IEICE and OSA.